MICHIGAN STATE UNIVERSITY

CYCLOTRON LABORATORY

NEUTRON SPECTRA AND LEVEL DENSITY PARAMETERS FROM THE $^{16}O + ^{12}C$ FUSION REACTION

J. KASAGI, B. REMINGTON, A. GALONSKY, F. HAAS,
J.J. KOLATA, L. SATKOWIAK, M. XAPSOS, R. RACCA,
and F.W. PROSSER

DECEMBER 1984

MSUCL-500

MSUCL 500
December 1984

Neutron Spectra and Level Density Parameters from the $^{16}O + ^{12}C$ Fusion Reaction

J. Kasagi*, B. Remington, A. Galonsky, and F. Haas+
Cyclotron Laboratory, Michigan State University,
East Lansing, Michigan 48824

J.J. Kolata, L. Satkowiak, and M. Xapsos
University of Notre Dame, Notre Dame, IN 46556

R. Racca@ and F.W. Prosser,
University of Kansas, Lawrence, KS 66045

Residues following $^{16}O + ^{12}C$ fusion were identified by their characteristic γ-rays. For several transitions in ^{23}Mg, ^{25}Mg, and ^{26}Al coincident neutron spectra were measured at six angles. Through use of the evaporation code CASCADE, comparisons were made of these spectra with predictions of the statistical model at five ^{16}O projectile energies between 43.2 and 56.0 MeV. The result requires an excitation energy dependence for the effective radius parameter r_o, which determines the spin cut off factor.

* While on leave from Tokyo Institute of Technology.
+ While on leave from University of Strasbourg.
@ Present address: Mission Research Corp., Colorado Springs, CO.

I. Introduction

The statistical model[1] has often been used to describe the decay of a highly excited nucleus. When that nucleus is formed by the collision of two heavy nuclei the excitation is enriched in high-spin states. In such cases[2,3] the model[4,5] has done a good job of predicting the distribution of evaporation residues when reasonable choices were made for level densities and yrast lines. Comparison to more specific measurements could, of course, provide a more severe test of the model or, at the least, more uniquely determine some of its parameters.

We have obtained data for such a test - a vast set of neutron spectra in coincidence with various γ-rays emitted in evaporation residues. We used one reaction - $^{16}O + ^{12}C$ - and used five ^{16}O bombarding energies from 43.2 MeV to 56.0 MeV, some of them "on" and some of them "off" the well-known resonances.[6,7] In three residues - ^{23}Mg, ^{25}Mg, and ^{26}Al - we could detect γ-rays in coincidence with neutrons which were observed at six angles. The resulting number of neutron spectra was 414, many with good statistical accuracy. Hence, we could compare these spectra with the predictions of the statistical model. For this purpose, with some modifications, we used the program of Pühlhofer, CASCADE.[5]

II. Experimental Method

The data were obtained at the University of Notre Dame, where beams of ^{16}O were produced in a three-stage electrostatic accelerator system. The target was a commercial carbon film of thickness 100 μg/cm^2. At 100 μg/cm^2 the total spread of reaction energy was about 1 MeV or about 0.5 MeV in the center-of-mass system. In order to reduce the Doppler broadening of γ-rays, the carbon target was put on a Pb backing just thick enough to stop the beam and recoiling heavy residues, and the Pb was pressed onto a 3 mm Cu plate which served to dissipate the heat of the beam. With this arrangement a beam of 2 mm diameter and of 6×10^{10}/sec intensity could be tolerated by the target. The

target ladder was electrically insulated so that we could monitor beam intensity and collect charge.

Just outside the target chamber, which was a 6 cm aluminum cylinder with 2 mm wall thickness, we placed a Ge(Li) detector at 125° to the beam direction. The volume of the Ge(Li) was 107 cm^3, and the distance of its front face from the target was 4 cm.

Each neutron detector consisted of a glass encapsulated cylinder of NE213 liquid scintillator coupled through a conical lucite light pipe to a 5-cm diameter RCA 8575 photomultiplier. The diameter of the NE213 cylinder was approximately 12.7 cm and its thickness approximately 7.6 cm. One of the neutron detectors was placed at 0° (average polar angle = 4°), three were in the plane defined by the beam and the Ge(Li) detector at angles of 31°, 60°, and 104°, and two were at 90° to that plane at polar angles of 50° and 90°. Each detector was about 65 cm from the target. In some runs the Ge(Li) was on the side of the beam opposite the neutron detectors at 31°, 60°, and 104°, and in other runs it was on the same side.

The time-of-flight method was used to measure neutron energy from the time difference between a Ge(Li) pulse and a scintillator pulse. Since the scintillator has comparable efficiencies for neutrons and for γ-rays, the γ-ray peak in the time-of-flight spectrum was quite apparent, and was used as a reference to determine absolute flight times, hence energies, for the neutrons. The width of the γ-ray peak, arising almost entirely from time jitter in the Ge (Li), was used to determine the instrumental resolution. Its standard deviation, ~1.7 ns, when combined in quadrature with a scintillator-length term, corresponds to an energy resolution of ±0.10 MeV for 1 MeV neutrons. At higher energies the resolution is worse, ±2.3 MeV at 10 MeV, for example; but such a resolution function is not unsuitable for measuring evaporation-type spectra. The energy-dependent neutron efficiency was computed with the code TOTEFF[8] modified[9] to apply to the scintillator NE213 and to employ more modern values of n-p and n-C cross sections. The efficiency rises rapidly from a threshold energy to a peak value

and then falls off slowly with further increase in neutron energy. In the rising portion the computed efficiency depends sensitively on the exact value of the threshold, on the luminous response of the scintillator, and on the pulse-height resolution of the scintillator. Therefore, although our thresholds were set at 1 MeV, we did not use data below 2 MeV. Even so, spectrum distortion between 2 and 4 MeV may be as high as 25%; above 4 MeV it is probably less than 10%. Near the center of our range, around 10 MeV, the efficiency is 25%.

All coincident Ge(Li) - neutron events were stored on tape. An event consisted of a Ge(Li) pulse height, a Ge(Li) - scintillator TAC (Time-to-Amplitude Converter) output, and a scintillator pulse height which, with router bits, served as the neutron detector identification signal. In order to reduce the γ-ray background (both prompt and time-uncorrelated) in the neutron spectra, commercial pulse-shape discriminators were used to eliminate most of the γ-ray pulses from the scintillator spectra.

A typical Ge(Li) pulse-height spectrum gated by any of the six neutron detectors is shown in Fig. 1; some of the more prominent peaks are indicated. A neutron time-of-flight (TOF) spectrum, when gated by the 830 keV γ-ray in ^{26}Al, as seen in Fig. 1, is shown in Fig. 2. Those prompt γ-rays that were allowed to pass through the n-γ pulse-shape discriminator form the small peak at the right-hand end of the spectrum. From this reference peak and the calibration of the TAC, neutron energies were determined; some energies are indicated on the figure. In producing the γ-ray gated neutron TOF spectrum of Fig. 2 three spectra were first produced, one for a gate over the 830 keV line and two for gates of half the width on either side of the 830 keV gate. The latter two were subtracted from the first in order to have a spectrum free of coincidences with higher-energy γ-rays via their Compton tails. The error bars on the points reflect this subtraction. From this net spectrum a time-uncorrelated background of accidental coincidences was then subtracted. Over

the region of the neutron peak this background was about 10% of the net true coincidences.

The γ-rays and bombarding energies for which neutron spectra were created by this procedure are listed in Table 1. In this table S and O denote "same" and "opposite" for whether the Ge(Li) was on the same or the opposite side of the in-plane neutron detectors. The two orientations were used in order to test whether or not there was a difference in the corresponding neutron spectra. In fact, no statistically significant difference could be discerned. In comparing with theory the two spectra were, therefore, combined into one. The origins of the γ-rays listed in Table 1 are given in the energy-level diagrams of Fig. 3.

III. Experimental Results

For comparison with the statistical model through the program CASCADE we constructed neutron energy spectra in the center-of-mass (CM) system of $^{16}O + ^{12}C$. First we had to construct laboratory-system energy spectra from the TOF spectra. The quantities required to convert a time spectrum to an energy spectrum are the TAC calibration in ns/channel, the centroid of the γ-ray peak (see Fig. 2), the flight path length, and the energy-dependent detector efficiency. Corresponding to the TOF spectrum of Fig. 2 is the neutron energy spectrum of Fig. 4.

We allowed a fair number of γ-ray pulses to pass through the n/γ discriminator and found that the value of the γ-ray centroid in the TOF spectrum had a slight dependence on the energy of the coincident γ-ray in the Ge(Li), the Ge(Li) pulse coming later at the lower energies. This does not affect the energy resolution of the corresponding energy spectra because in generating TOF spectra we gated on individual γ-ray lines in the Ge(Li) spectrum. Since the time resolution is greater than the decay

time, even for the 585 keV state of ^{25}Mg, we could not observe a decay curve in the γ-ray peak, and no correction was made for it.

When a neutron spectrum at a fixed angle in the laboratory system, such as the one in Fig. 4, is transformed into a spectrum in the CM system, that spectrum is spread over a range of angles. If the CM angular distribution is isotropic, a spectrum measured at a single laboratory angle is sufficient to define the spectrum in the CM system; otherwise several angles are necessary. Our data were obtained at six laboratory angles. In principle we would then have six CM angles for any neutron energy. For one bombarding energy, 43.2 MeV, a set of neutron angular distributions in the CM system is given in Fig. 5. These neutrons are only those in coincidence with 417-keV γ-rays. Similar sets of angular distributions were obtained for neutrons gated by the eight other γ-rays and for all five bombarding energies, i.e., for the 39 combinations listed in Table 1. We see in Fig. 5, however, that the lab-to-CM transformation has produced six points only at the higher CM neutron energies. For $E_n \leq 0.95$ MeV, no angular distribution is available since only the 0° detector can detect neutrons which have such low energies in the CM system. We assumed isotropic distributions for such neutrons, since the angular distributions for the next few higher neutron energies are consistent with isotropic emission. Higher energy neutrons show definite deviation from an isotropic angular distribution. Legendre polynomial fits to the data using even terms up to $P_4(\cos\theta)$ have been made in order to obtain angle-integrated spectra for each energy in the CM system. The solid lines drawn in Fig. 5 are the results of these fits.

In making the above transformation from the lab system to the center-of-mass system we assumed that the neutron was emitted from ^{28}Si. Figure 7 shows, however, that for the residues detected in this experiment, ^{26}Al, ^{25}Mg and ^{23}Mg, all neutron channels contain at least one charged particle. If a charged particle is emitted before the neutron, the source velocity is no longer the velocity of the fused ^{28}Si nucleus (due to the recoil from the charged particle emission). It is impossible to make

the correct transformation because we do not know the energy-angle distributions of the charged particles and we do not know how often the charged particles are emitted first. However, to see the magnitude of this recoil effect on the neutron spectra, we used CASCADE to calculate theoretical spectra with and without the recoil correction, i.e., with and without an ^{27}Al source velocity added to the neutron velocities. The results are displayed in Fig. 6 for the final state nucleus ^{26}Al. The solid curve is the calculation without the recoil correction, corresponding to the assumption that the velocity of ^{27}Al is the same as that of ^{28}Si. (This same assumption was used in obtaining the CM energy spectra from the experimental lab spectra.) The dashed curve assumes a 4 MeV proton was emitted before the neutron with an isotropic angular distribution in the ^{28}Si rest frame, while the dotted curve corresponds to a 7 MeV proton. Since the average proton energy for the final nucleus of ^{26}Al is about 4 MeV, we would expect the dashed curve to be closest to the truth. From comparison of these curves, the effect of neglecting the recoil correction causes a 15% lower yield for E_n = 10 MeV. The effect is less than 5% for $E_n \leq 7$ MeV. Thus, with sufficient accuracy the analysis without the recoil correction can be applied for the present experiment.

In Figs. 8-13 are shown the angle-integrated neutron energy spectra in the CM system gated by γ-rays in ^{26}Al. Spectra gated by γ-rays in ^{23}Mg and ^{25}Mg are shown in Figs. 14 and 15, respectively. In these figures the bin widths in the energy spectra were chosen to reflect the energy resolution.

IV. Statistical Model Calculation

The program CASCADE written by Pühlhofer[2] was used to calculate the neutron spectra from the $^{16}O + ^{12}C$ system. As the details of the program are described in Ref. 2, only the parameters used in the present calculations are described here. For a given system, the fusion reaction cross section can be parameterized by

$$\sigma_f = \pi\lambda^2 \sum_{\ell=0}^{\infty} (2l+1)T_\ell$$

where

$$T_\ell = \frac{1}{1 + \exp((\ell-\ell_0)/d)}$$

is the transmission coefficient, ℓ_0 is the angular momentum cutoff parameter, and "d" is the diffuseness parameter. Since the fusion reaction cross sections of the $^{12}C + ^{16}O$ system have been measured at the incident energies of the present experiment[3], ℓ_0 was chosen so as to reproduce the experimental σ_f with a diffuseness of d = 1. The calculated shapes of the neutron spectra are quite insensitive to changes of up to 3 in both "d" and ℓ_0. The emitted particles considered in the calculation are neutron, proton, α-particle and γ-ray. Transmission coefficients of the evaporated particles were calculated from optical model potentials of Wilmore and Hodgson[10] for neutrons, of Perey[11] for protons, and of Satchler[12] for α-particles. The reduced γ-ray transition strengths used in the calculation were 0.001 W.u., 0.05 W.u. and 5 W.u. for E1, M1, and E2 transitions, respectively.

In the program, excitation energies are divided into four regions and different level density parameters can be used for each region. For the lowest excitation energies (region I), the known levels compiled by Endt and Van der Leun[13] are used with their spins and parities for each nucleus. For the next region (region II), the level density parameters "a" (the usual level density parameter) and Δ (the pairing energy or virtual ground state position) have been reparameterized by Pühlhofer[2], using the compilations of Vonach and Hille[14] and of Dilg et al.[15] These parameterizations are built into the program. The parameter values used for the present calculations are listed in Table 2 for each nucleus. For the highest excitation energies (region IV), where the shell effects on the level density are considered to disappear,[16] the parameter "a" is assumed to have

the form A/constant (A is the mass number) and the constant is treated as a free parameter and fitted to the experimental data. The parameter Δ used in this region is calculated from the assumption that the virtual ground state for the level density in this region should coincide with the ground state energy of a spherical liquid drop.[16] The parameter values in region IV are also listed in Table 2. For region III, which corresponds to the region between II and IV, the program interpolates the level density parameters linearly. In summary, region I is the low excitation energy region where the levels are known. Region II extends from region I to 10 MeV, region III is from 10 MeV to 20 MeV, and region IV is from 20 MeV and above. The effective radius parameter r_0, which determines the spin cutoff factor, is also fitted to the data as a free parameter. Thus, there are only two input parameters to be varied in comparing the calculation to the experimental data. One of them is the level density parameter "a" in region IV and the other is the effective radius parameter r_0.

For evaporated particles the program provides energy spectra which have been obtained by integrating over angle and by summing over all the decay steps from the initial compound nucleus to the final evaporation residue. In the present experiment, however, neutron spectra gated by specific γ-rays were measured. In order to compare the calculation with the present experiment, the following calculation was carried out with a modified version of CASCADE.

First, we define "sticking probability" for a channel as the probability that once the channel is entered it decays further, but only by γ-ray emission. Then the procedure we followed to predict exclusive spectra with CASCADE is as follows (see Fig. 7): For the case when ^{26}Al is the residue, neutrons are emitted either from ^{28}Si or from ^{27}Al. In the latter case, we need only weight the neutron spectrum by the sticking probability for ^{26}Al (since we detect a residue-identifying coincident γ-ray in the Ge(Li) detector). For the neutrons emitted by ^{28}Si, we first have to weight the spectrum by the branching ratio for proton

emission out of ^{27}Si. This is then further weighted by the "sticking probability" for ^{26}Al. The above weighting is carried out as a function of excitation energy and angular momentum (J) using the population matrix and the decay probability of each nucleus, both of which are provided by CASCADE. Similarly, we calculate exclusive neutron spectra for the residues ^{25}Mg and ^{23}Mg.

In this calculation, a "gate" on spin and excitation energy of the residue is set via the sticking probability matrix. In the present calculations, for the neutron spectra gated by the 3918 keV γ-ray ($7^+ \rightarrow 5^+$) in ^{26}Al only the region with $J \geq 7$ is selected. For those spectra gated by other γ-rays in ^{26}Al, yrast state populations are excluded from the matrix, and for those gated by γ-rays in ^{23}Mg the ground state population is excluded.

V. Comparison with the calculation.

First we compared theory with experiment for the neutron spectra gated by the 417 keV γ-ray in ^{26}Al. The parameters "a" and r_0 are obtained so as to give the best fits to these spectra; spectra gated by other γ-rays in ^{26}Al have poorer statistical accuracy. Results of the comparison are shown in Fig. 8 for both E_i = 46.0 and 56.0 MeV. The calculated spectra are normalized arbitrarily since the absolute yield has not been measured in the present experiment.

As can be seen in the upper half of the figure, the slope of the high energy side of the calculated spectra is very sensitive to "a", while the lower half shows that the behavior of the low energy part of the spectra is mainly determined by r_0. The calculations for a = A/8, A/9, and A/10 are shown in Fig. 8(a) with dotted, solid and dashed lines, respectively. Although the value of a=A/8 reproduces the data reasonably well, the value of a = A/9 fits the data better between 3 and 7 MeV for all the incident energies. In Fig. 8(b) are shown the calculations with various values of r_0. Dashed, dotted, solid and dot-dashed curves show those with r_0 = 1.8 fm, 1.7 fm, 1.6 fm, and 1.5 fm,

respectively. The calculation with r_0=1.6 fm reproduces the data for lower incident energies. To reproduce the data at higher incident energy (E_i=53.8 and 56.0 MeV), larger values of r_0 are required, as seen in the figure. Varying the boundary between regions III and IV does not eliminate this dependence of r_0 on the incident energy. A change of the assumed γ-ray transition strengths makes only slight changes in the neutron spectra. For example, changing those values by a factor of 10 either way makes a 5% change in the slope of the spectra. The final values of r_0 obtained in the comparisons with the experimental data are 1.6 fm for E_i=43.2, 46.0, and 48.3 MeV, 1.7 fm for E_i=53.7 MeV and 1.8 fm for E_i=56.0 MeV.

The spectra gated by other γ-rays are shown in Figs. 9-15 along with the calculations. Only by using the above r_0 values for each incident energy can the calculation reproduce the neutron spectra in different decay channels.

Although still within the energy uncertainty of the data, the highest energy points in the spectra are systematically higher than the calculations. This larger than expected yield of the high energy neutrons might be caused by processes other than evaporation from the fully equilibrated system that CASCADE assumes to exist at the start.

VI. Discussion

As can be seen in Figs. 8-15, the statistical model calculation can reproduce the neutron energy spectra from the ^{12}C + ^{16}O reaction over a wide range of incident energies. We could see no effect of the incident energy being either "on" or "off" a resonance.[6,7] The value of A/9.0 for "a" in region IV obtained in the present analysis turns out to be almost the same as the value of "a" in region II for each nucleus, as shown in Table 2. Therefore, the present results do not give evidence for the existence of a region of high excitation energy (region IV) where the shell effects on the level density disappear.

On the other hand, the constraint of fitting the neutron spectra for each incident energy clearly requires a dependence on incident energy of the effective radius parameter r_0. Of particular interest is the fact that larger values of r_0 are required for higher incident, and therefore, higher excitation energies. A larger r_0 serves to increase the density of high spin states in the sequentially decaying nuclei, and thereby it enhances the low energy neutron yield. The values of r_o obtained in the present work are much larger than those determined at lower excitation energies. The value of $r_o \approx 1.25$ fm has been widely used to obtain the level density parameters from experimental data.[14,15,17] It has been pointed out[18], however, that the value of $r_o = 1.4$ fm was deduced from a shell model calculation for an average value of the square of the projection of the total angular momentum for the states around the Fermi level. At high excitation energies, little information about the level density has been available so far. In this mass region, the $^{12}C(^{14}N,^{6}Li)^{20}Ne$ reaction has been studied with a statistical model analysis.[19,20] The absolute cross sections to discrete low-lying states in ^{20}Ne were compared with calculations, and their results also required larger values of the radius parameter, namely r_0=1.5 fm[19] and r_0=1.6 fm.[20]

Recently, the level density has been calculated with shell model single particle levels.[21] For the high excitation energy region, the result shows drastic deviation from the level density obtained by the parameterization at low excitation energies based on the Fermi gas model. The calculated spin dependence of the level density seems to require an excitation energy dependence of the spin cutoff parameter when the conventional level density parameterization is applied to fit them. Thus, it is highly desirable to systematically obtain level density information for the high excitation energy and high spin region. The present method is very useful for such a purpose, since neutrons are free from the Coulomb barrier and the whole spectrum (including the low energy neutrons) directly reflects the level densities of the sequentially decaying nuclei.

Two of us (J.K. and F.H.) wish to thank the Cyclotron Laboratory for its kind hospitality during our stays.

References

1. W. Hauser and H. Feshbach, Phys. Rev. 87, 366 (1952) and H. Feshbach in Nuclear Spectroscopy, F. Ajzenberg-Selove, part B, p. 625 (1960).

2. F. Pühlhofer, Nucl. Phys. A280, 267 (1977).

3. J.J. Kolata, R.M. Freeman, F. Haas, B. Heusch, and A. Gallmann, Phys. Rev. C 19, 408 (1979).

4. Computer code CASCADE by F. Pühlhofer, April 1980 version.

5. Monte Carlo code LILITA by J.G. del Campo and R.G. Stokstad.

6. P. Sperr, S. Vigdor, Y. Eisen, D.G. Kovar, T.R. Ophel, and B. Zeidman, Phys. Rev. Lett. 36, 405 (1976).

7. J.J. Kolata, R.M. Freeman, F. Haas, B. Heusch, and A. Gallman, Phys. Lett. 65B, 333 (1976).

8. R.J. Kurz, UCRL Report 11339, Berkeley, California (1964).

9. R.R. Doering, Ph.D. Thesis, Michigan State University, 1974.

10. D. Wilmore and P.E Hodgson, Nucl. Phys. 55, 673 (1964).

11. F.G. Perey, Phys. Rev. 131, 745 (1963).

12. G.R. Satchler, Nucl. Phys. 70, 177 (1965).

13. P.M. Endt and C. Van der Leun, Nucl. Phys. A310, 1 (1978).

14. H. Vonach and M. Hille, Nucl. Phys. A127, 289 (1969).

15. W. Dilg, W. Schantl, H. Vonach and M. Uhl, Nucl. Phys. A217, 269 (1973).

16. V.S. Ramamurthy, S.S. Kapoor and S.K. Kataria, Phys. Rev. Lett. 25 (1970) 386; F.C. Williams,Jr., G. Chan and J.R. Huizenga, Nucl. Phys. A187, 225 (1972).

17. A. Gilbert and A.G.W. Cameron, Can. J. of Phys. 43, 1446 (1965).

18. U. Facchini and E. Saetta-Menichella, Energ. Nucl. 15, 54 (1968).

19. D.L. Hanson, R.G. Stokstad, K.A. Erb, C. Olmer and D.A. Bromley, Phys. Rev. C 9, 929 (1974).

20. C. Volant, M. Conjeaud, S. Harar, S.M. Lee, A. Lepine and E.F. DaSilveira, Nucl. Phys. A238, 120 (1975).

21. M. Ohta, K. Hatogai, S. Okai and Y. Abe, Phys. Rev. C 29, 1948 (1984).

Table 1. Bombarding energies and γ-ray energies for which we have neutron spectra. S and O refer to the orientation of the Ge(Li) detector with respect to that of the three in-plane neutron detectors--i.e., to whether it was on the same or opposite side of the beam. The numbers in the first column are the bombarding energies in MeV. The numbers in the second row are the γ-ray energies in keV.

E_i	^{23}Mg		^{25}Mg		^{26}Al				
	451	1600	585	975	417	830	1011	1623	3918
43.2	S,O	S,O			S,O	S,O	S,O	S,O	S,O
46.0	S,O	S,O			S,O	S,O	S,O	S,O	S,O
48.0	S,O	S,O			S,O	S,O	S,O	S,O	S,O
53.7	O	O	O	O	O	O	O	O	O
56.0	S,O	S,O	S,O	S,O	S,O	S,O	S,O	S,O	S,O

Table 2. Level density parameters "a" (in MeV^{-1}) and pairing energies Δ (in MeV) used in the calculation.

		^{28}Si	^{27}Si	^{27}Al	^{26}Al	^{25}Na	^{24}Mg	^{23}Mg
Region II ($E_x \leq 10$ MeV)	a	2.98	3.05	3.05	2.95	2.86	2.61	2.66
	Δ	1.82	-1.09	-1.09	-2.46	-1.06	2.07	-1.02
Region IV ($E_x \geq 20$ MeV)	a	3.11	3.0	3.0	2.89	2.78	2.67	2.56
	Δ	4.02	-1.16	-0.03	-2.24	-3.04	2.55	-2.17

Figure Captions

Fig. 1. Neutron-gated Ge(Li) pulse-height spectrum. Some of the observed γ-ray transitions in the residues ^{26}Al and ^{23}Mg are indicated.

Fig. 2. Neutron-Ge(Li) time-of-flight spectrum gated by the 830 keV γ-ray transition in the residue ^{26}Al. The neutron detector was at 0° to the beam. The small γ-ray peak on the right side of the spectrum serves as the reference for the transformation from time to energy. Neutron lab energies are indicated at the top.

Fig. 3. The observed γ-ray transitions in the three neutron channels studied, i.e., ^{12}C(^{16}O, pn)^{26}Al, ^{12}C(^{16}O,αn)^{23}Mg, and ^{12}C(^{16}O,2pn)^{25}Mg. Listed on the left is the energy and on the right the spin, parity, and half-life of each level.

Fig. 4. The laboratory energy spectrum corresponding to the TOF spectrum of Fig. 2.

Fig. 5. Angular distributions of neutrons in the CM system for beam energy of 43.2 MeV. Along the righthand vertical axis are listed the neutron energies in MeV.

Fig. 6. Calculated neutron spectra in the CM system with and without recoil correction. The solid line is the calculation without any recoil correction. The dashed curve includes recoil for 4 MeV protons emitted isotropically and before the neutron. The dotted curve is for 7 MeV protons. The beam energy is assumed to be 53.7 MeV and the residue is ^{26}Al.

Fig. 7. The decay scheme for ^{28}Si showing the channels leading to the residues observed, viz. ^{25}Mg, ^{26}Al and ^{23}Mg.

Fig. 8. Calculated neutron spectra compared to the experimental spectra for various values of the radius parameter r_o and the level density parameter "a" in region IV for the residue ^{26}Al. (a) Top spectrum is for 56 MeV beam energy and r_o = 1.8 whereas the lower spectrum is for 46 MeV incident energy and r_o = 1.6. In both cases, the dashed line is for a = A/10, solid line for a = A/9, and dotted line for a = A/8.
(b) Top curve is for 56 MeV incident energy and the bottom curve for 46 MeV. The value of "a" in region IV is A/9. The dashed curve is the calculation for r_o = 1.8, dotted for r_o = 1.7, solid for r_o = 1.6, and dot-dashed for r_o = 1.5.

Fig. 9. The experimental spectra compared to calculation for the five γ-ray transitions observed in the final state nucleus ^{26}Al at 43.2 MeV incident energy. The calculation uses r_o=1.6 fm, and the energy of the coincident γ-ray is listed by each spectrum.

Fig. 10. Same as Fig. 9 except that the incident energy is 46.0 MeV.

Fig. 11. Same as Fig. 9 except that the incident energy is 48.3 MeV.

Fig. 12. Same as Fig. 9 except that the incident energy is 53.7 MeV and r_o = 1.7 fm in the calcuation. The calculation with r_o = 1.6 fm is shown by a dashed line.

Fig. 13. Same as Fig. 9 except that the incident energy is 56.0 MeV and r_o = 1.8 fm in the calculation. The calculation with r_o = 1.6 fm is shown by a dashed line.

Fig. 14. Experimental and calculated spectra for the final state nucleus ^{23}Mg. The energies of the incident ^{16}O and of the coincident γ-rays are listed to the right of the spectra. In the

calculation r_o = 1.6 fm for E_i = 43.2, 46.0, and 48.3 MeV, 1.7 fm for E_i = 53.7 MeV, and 1.8 fm for E_i = 56.0 MeV.

Fig. 15. Same as Fig. 14 except that the residue is ^{25}Mg, and there are data for only the two highest incident energies.

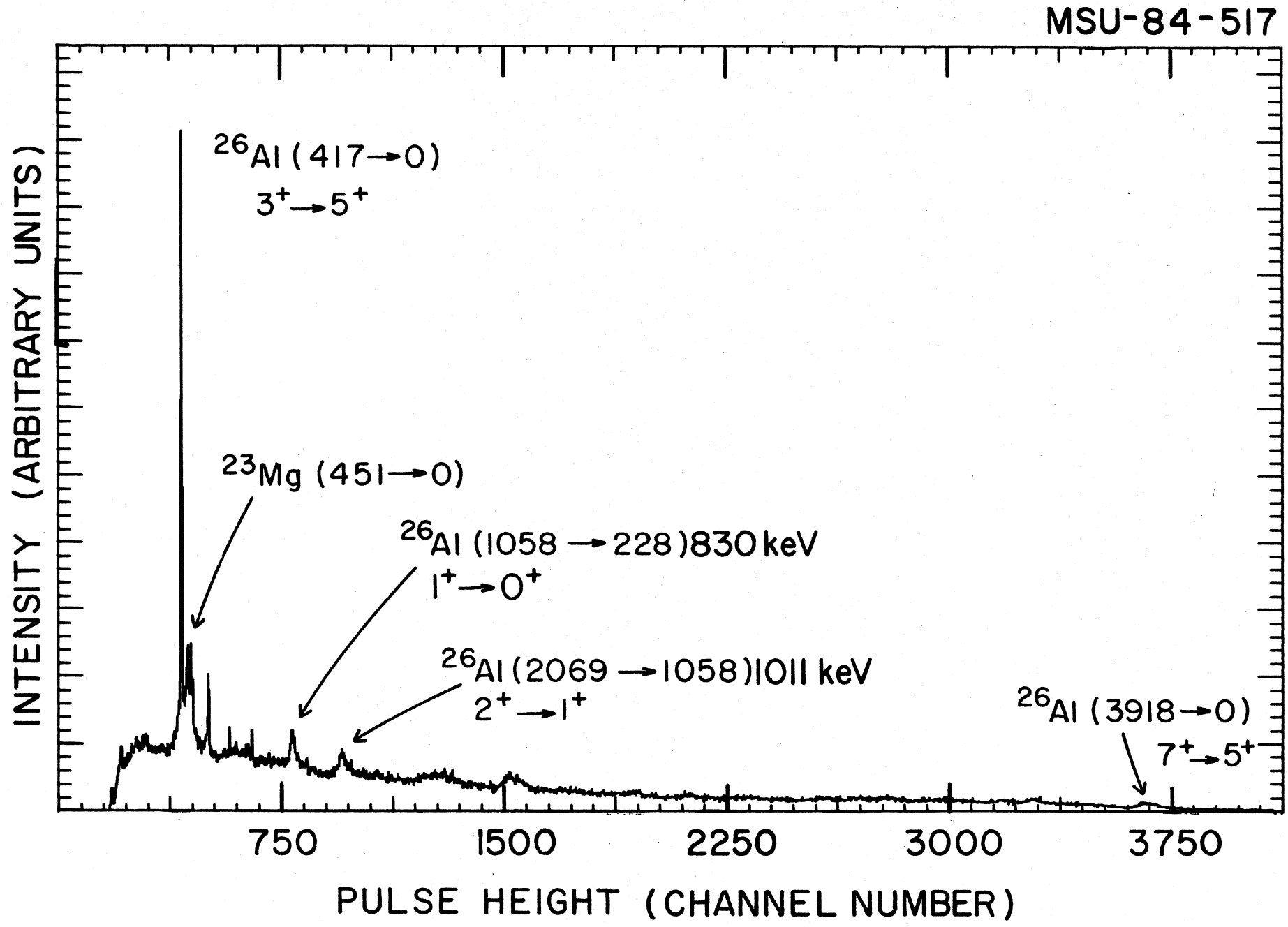
MSU-84-517
INTENSITY (ARBITRARY UNITS)
^{26}Al (417→0)
3$^+$→5$^+$
^{23}Mg (451→0)
^{26}Al (1058 → 228) 830 keV
1$^+$→0$^+$
^{26}Al (2069 → 1058) 1011 keV
2$^+$→1$^+$
^{26}Al (3918→0)
7$^+$→5$^+$
750
1500
2250
3000
3750
PULSE HEIGHT (CHANNEL NUMBER)

MSU-84-520

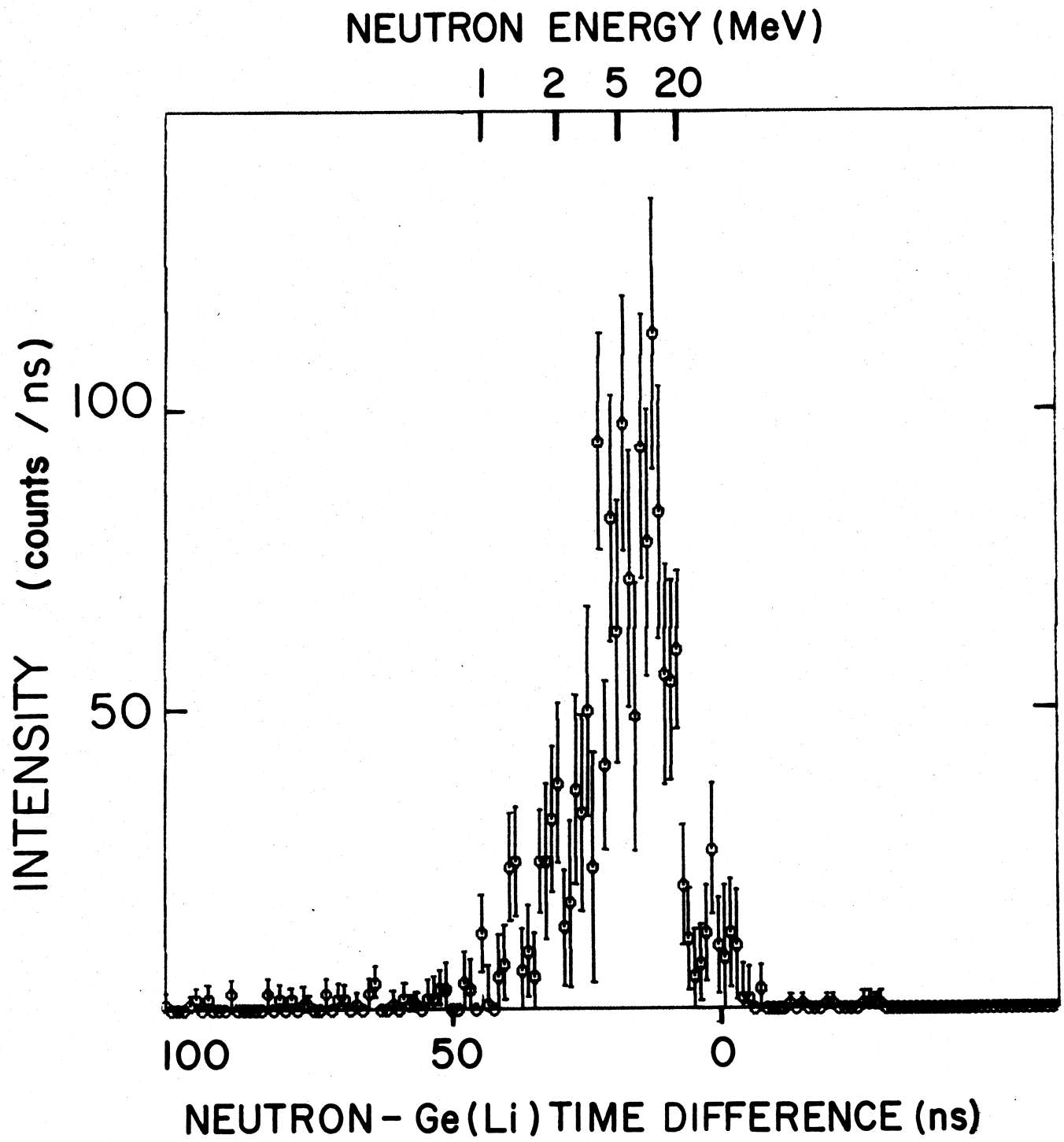
NEUTRON ENERGY (MeV)
1
2
5
20
INTENSITY (counts / ns)
100
50
100
50
0
NEUTRON - Ge(Li) TIME DIFFERENCE (ns)

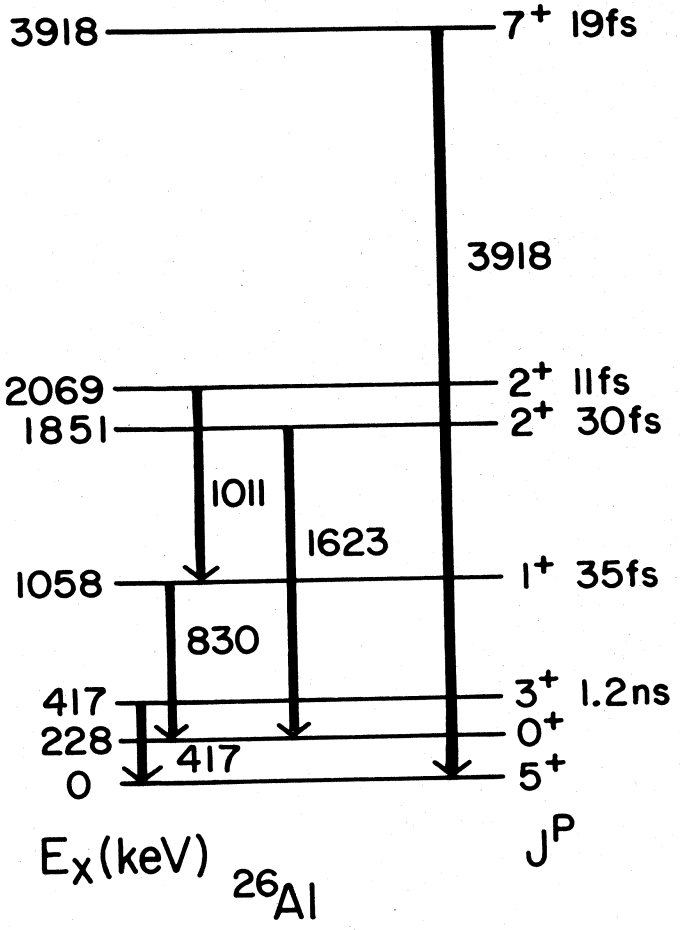
3918
7+ 19fs
3918
2069
2+ 11fs
1851
2+ 30fs
1011
1623
1058
1+ 35fs
830
417
3+ 1.2ns
228
0+
417
0
5+
Ex(keV)
26Al
JP

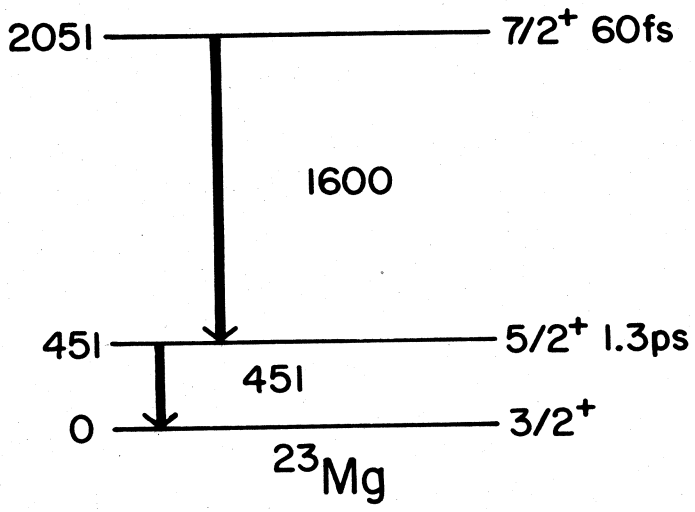
2051
7/2+ 60fs
1600
451
5/2+ 1.3ps
451
0
3/2+
23Mg

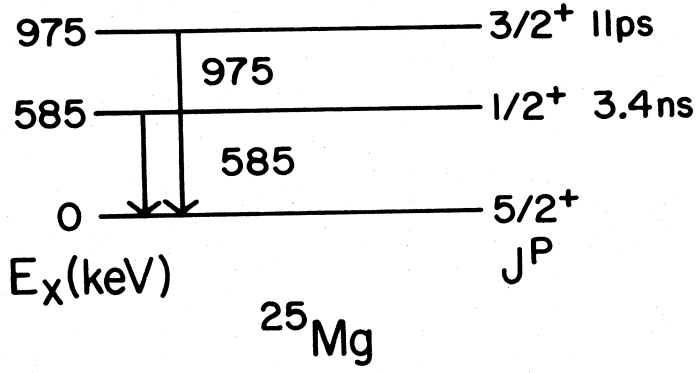
975
3/2+ 11ps
975
585
1/2+ 3.4ns
585
0
5/2+
Ex(keV)
JP
25Mg

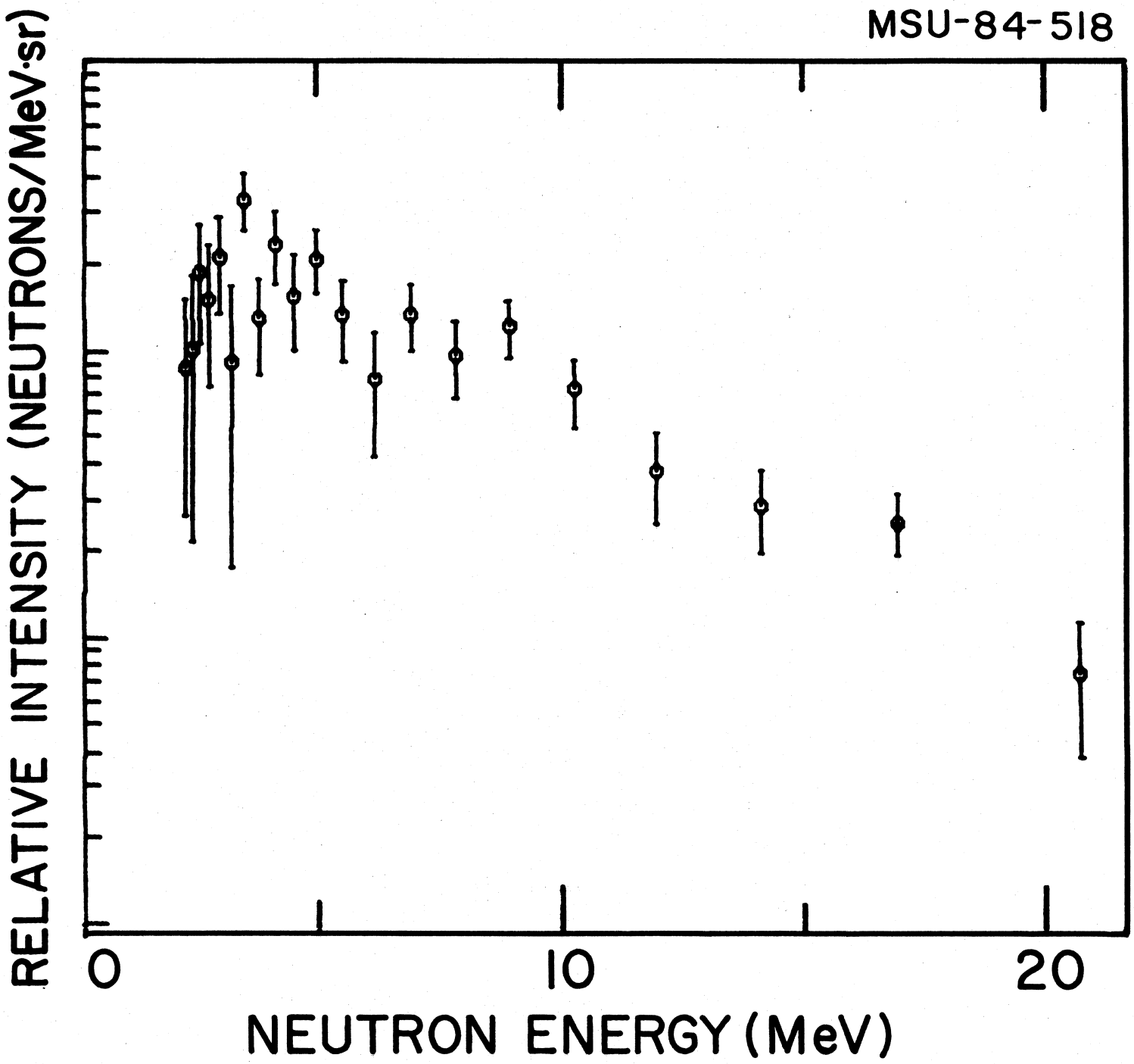
MSU-84-518
RELATIVE INTENSITY (NEUTRONS/MeV·sr)
0
10
20
NEUTRON ENERGY (MeV)

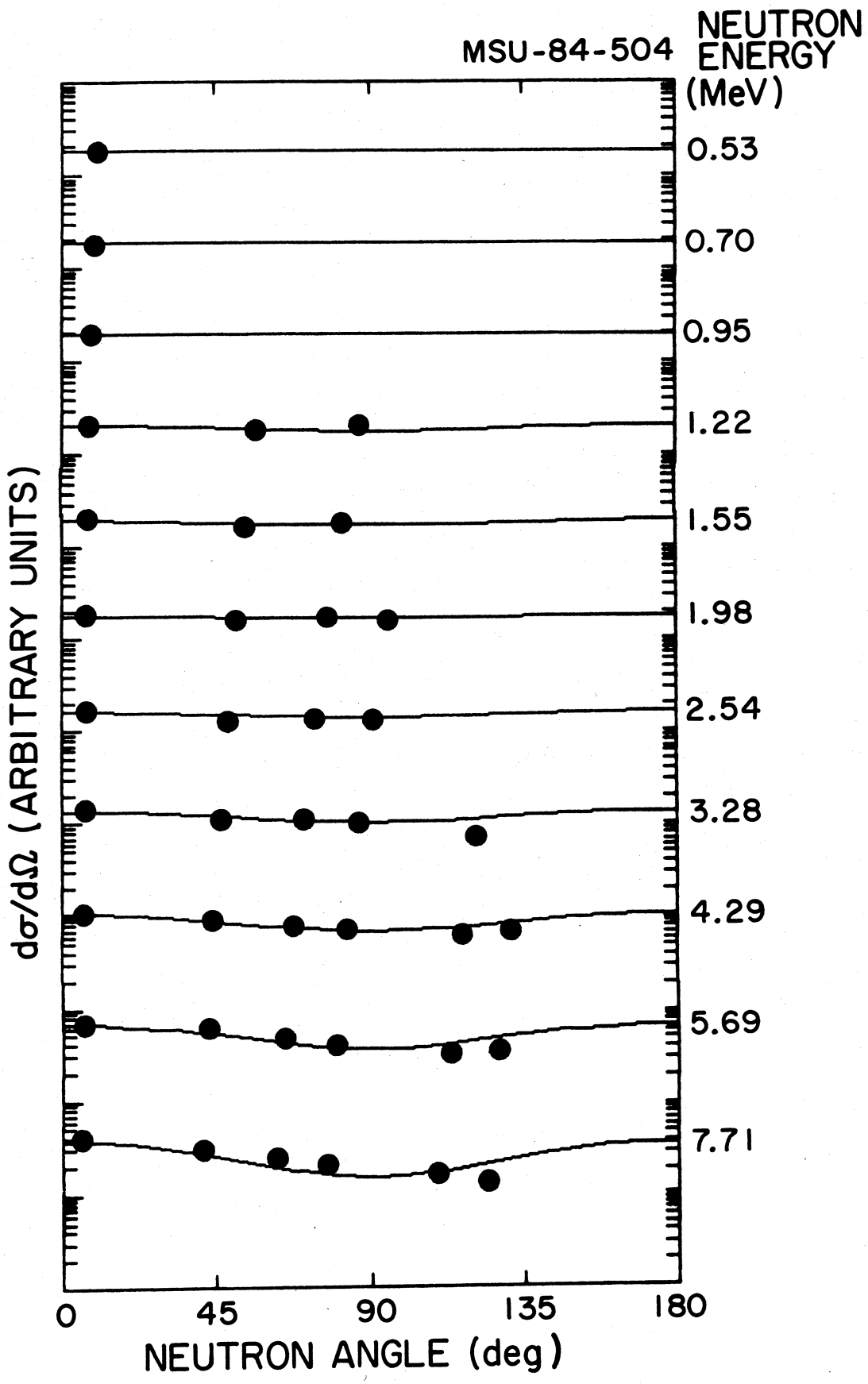
MSU-84-504
NEUTRON ENERGY (MeV)
0.53
0.70
0.95
1.22
1.55
1.98
2.54
3.28
4.29
5.69
7.71
dσ/dΩ (ARBITRARY UNITS)
0
45
90
135
180
NEUTRON ANGLE (deg)

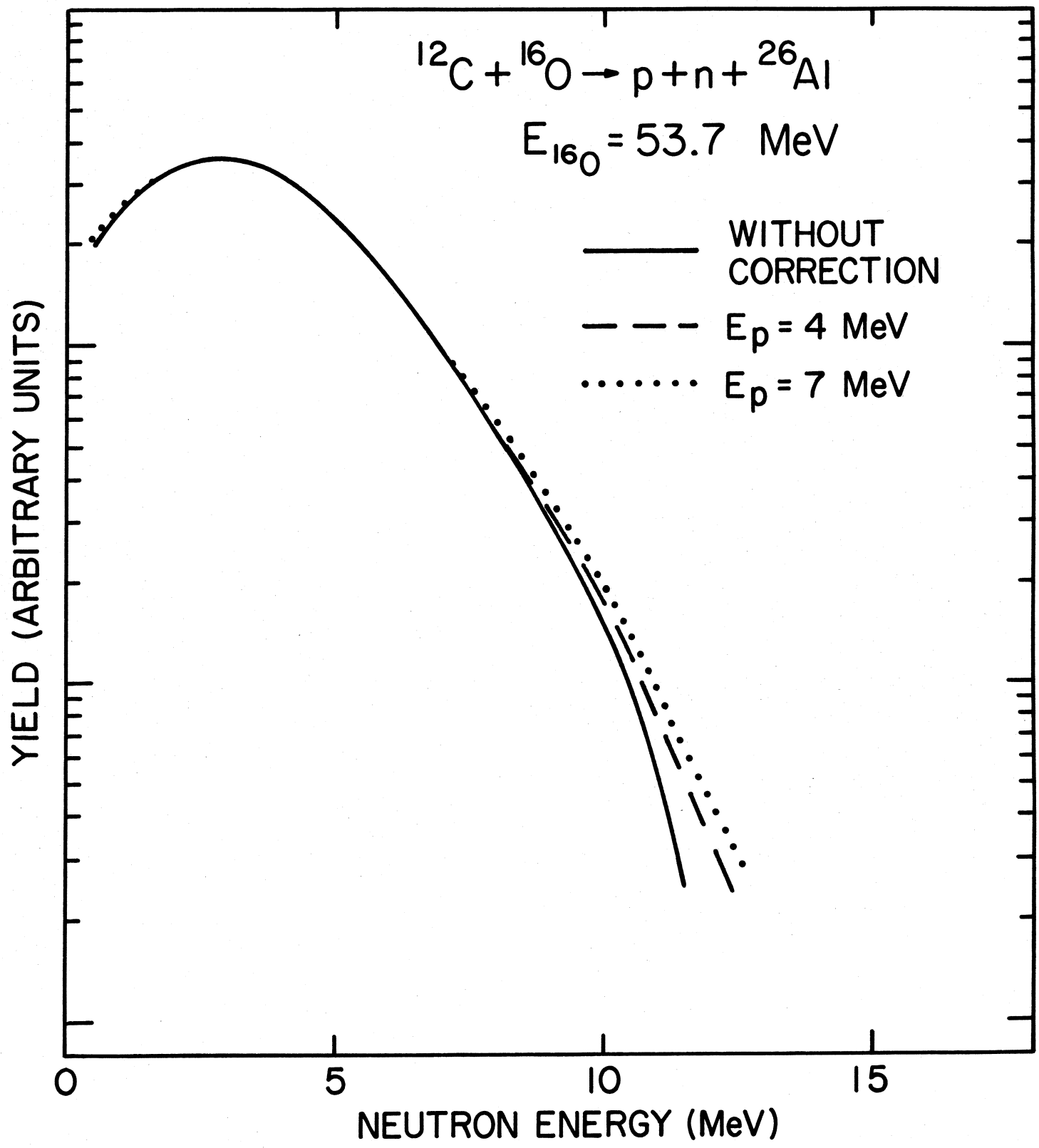
$^{12}C + ^{16}O \rightarrow p + n + ^{26}Al$
$E_{^{16}O} = 53.7$ MeV
WITHOUT CORRECTION
$E_p = 4$ MeV
$E_p = 7$ MeV
YIELD (ARBITRARY UNITS)
0
5
10
15
NEUTRON ENERGY (MeV)

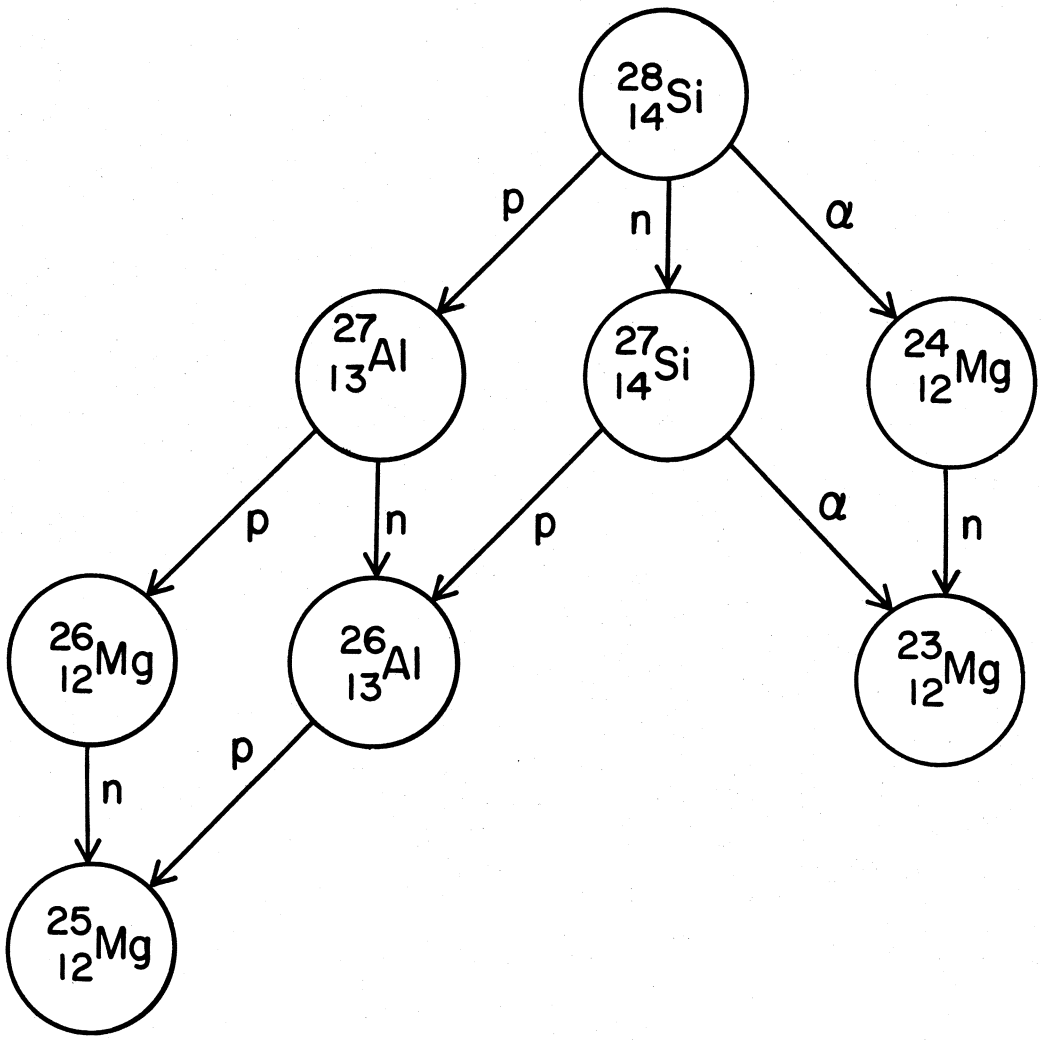
$^{28}_{14}Si$
p
n
α
$^{27}_{13}Al$
$^{27}_{14}Si$
$^{24}_{12}Mg$
p
n
p
α
n
$^{26}_{12}Mg$
$^{26}_{13}Al$
$^{23}_{12}Mg$
p
n
$^{25}_{12}Mg$

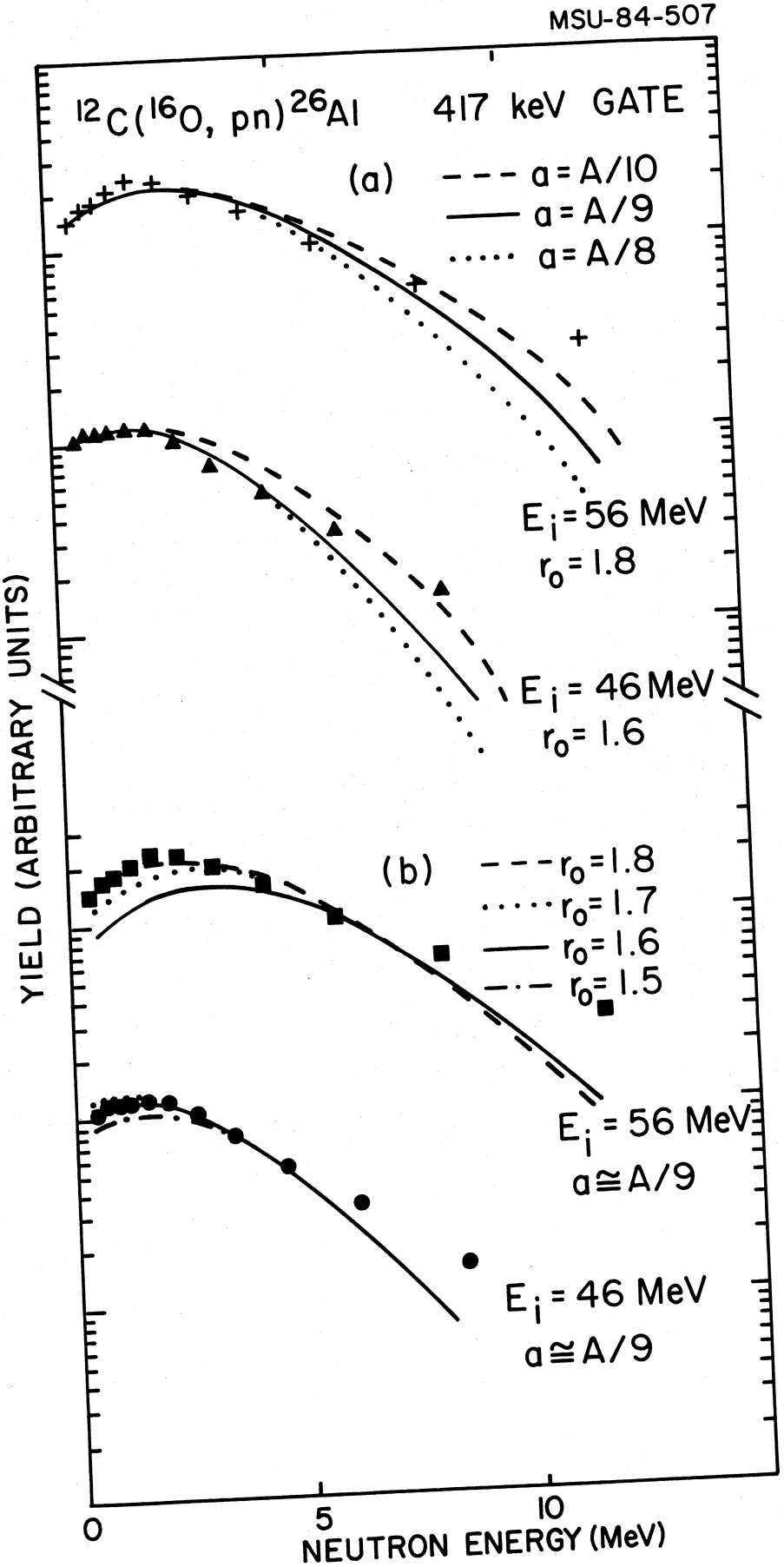
$^{12}C(^{16}O, pn)^{26}Al$ 417 keV GATE
(a)
--- a = A/10
—— a = A/9
····· a = A/8
E_i = 56 MeV
r_0 = 1.8
E_i = 46 MeV
r_0 = 1.6
(b)
--- r_0 = 1.8
····· r_0 = 1.7
—— r_0 = 1.6
-·- r_0 = 1.5
E_i = 56 MeV
a ≅ A/9
E_i = 46 MeV
a ≅ A/9
YIELD (ARBITRARY UNITS)
0
5
10
NEUTRON ENERGY (MeV)

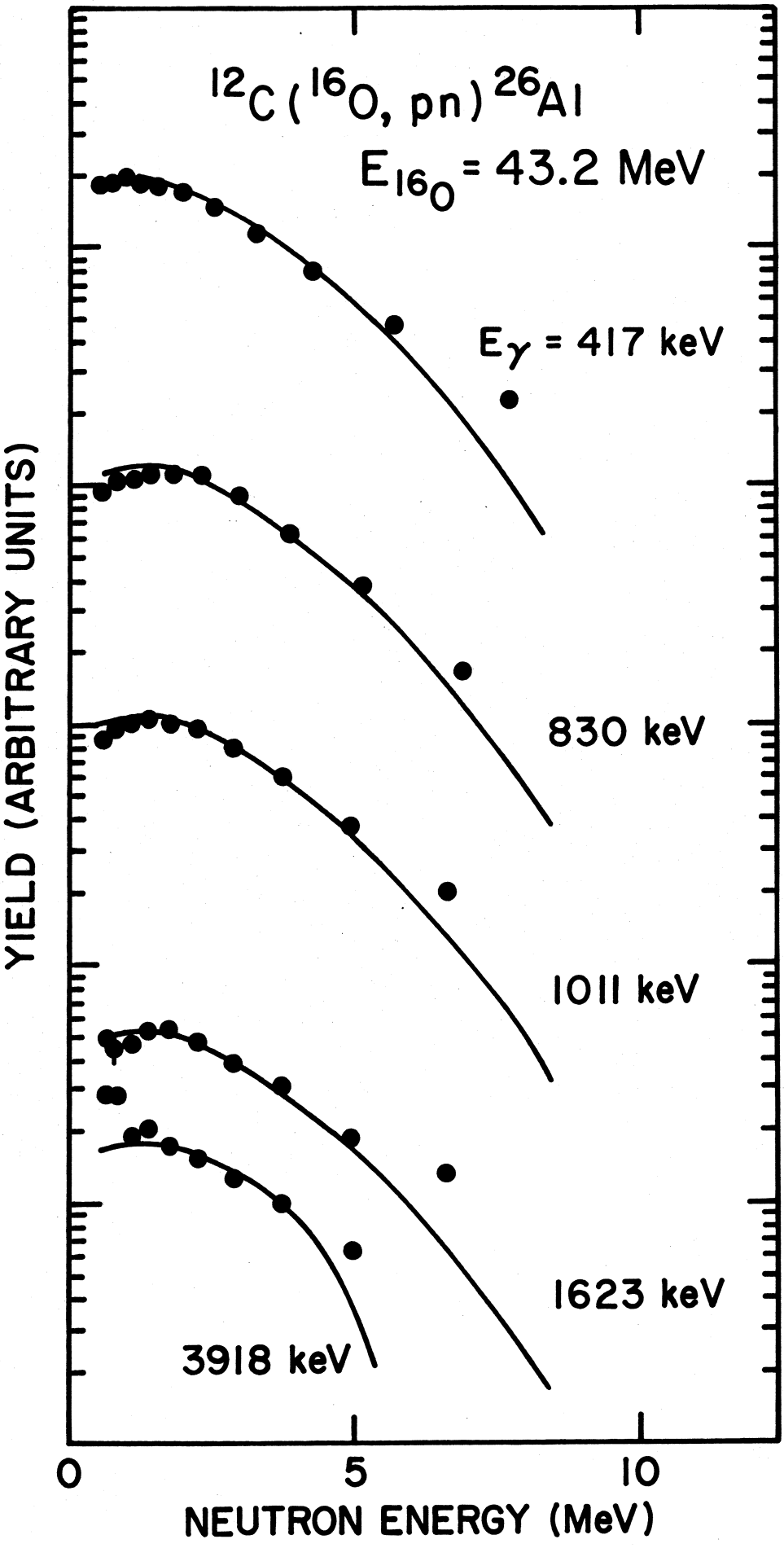
$^{12}C(^{16}O, pn)^{26}Al$
$E_{^{16}O} = 43.2$ MeV
$E_\gamma = 417$ keV
830 keV
1011 keV
1623 keV
3918 keV
YIELD (ARBITRARY UNITS)
0
5
10
NEUTRON ENERGY (MeV)

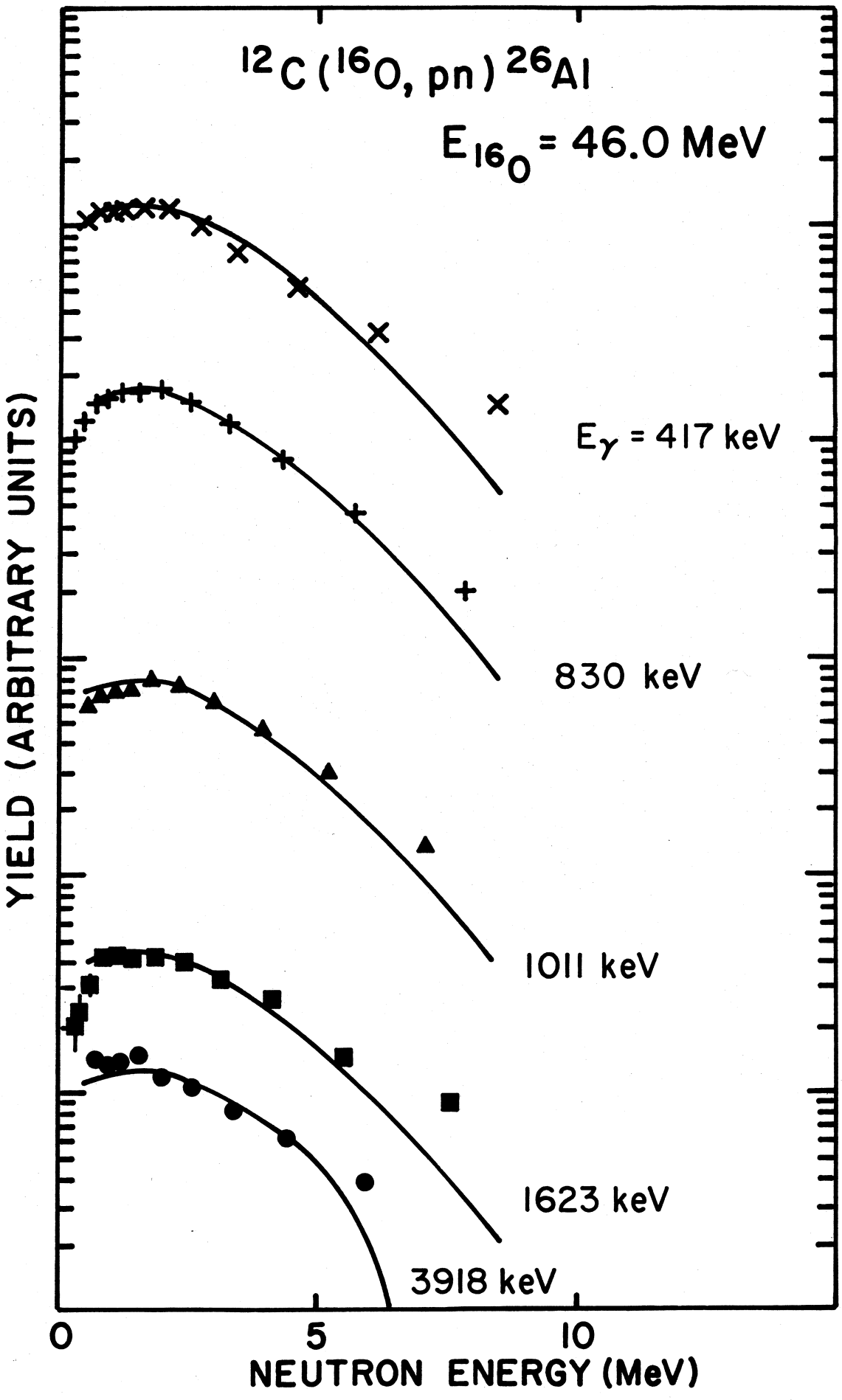
$^{12}C(^{16}O, pn)^{26}Al$
$E_{^{16}O}$ = 46.0 MeV
E_γ = 417 keV
830 keV
1011 keV
1623 keV
3918 keV
YIELD (ARBITRARY UNITS)
0
5
10
NEUTRON ENERGY (MeV)

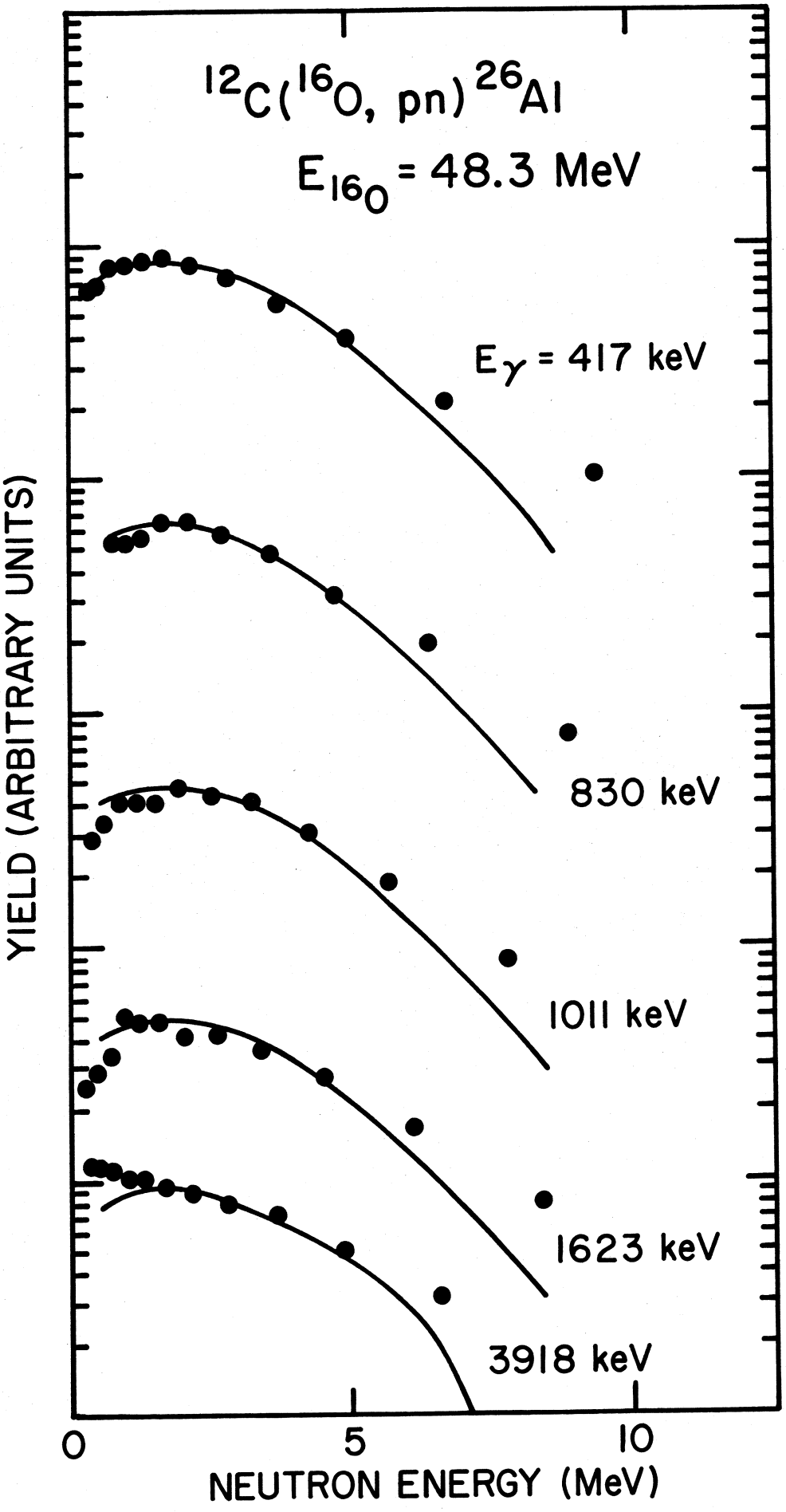
$^{12}C(^{16}O, pn)^{26}Al$
$E_{^{16}O} = 48.3$ MeV
$E_\gamma = 417$ keV
830 keV
1011 keV
1623 keV
3918 keV
YIELD (ARBITRARY UNITS)
0
5
10
NEUTRON ENERGY (MeV)

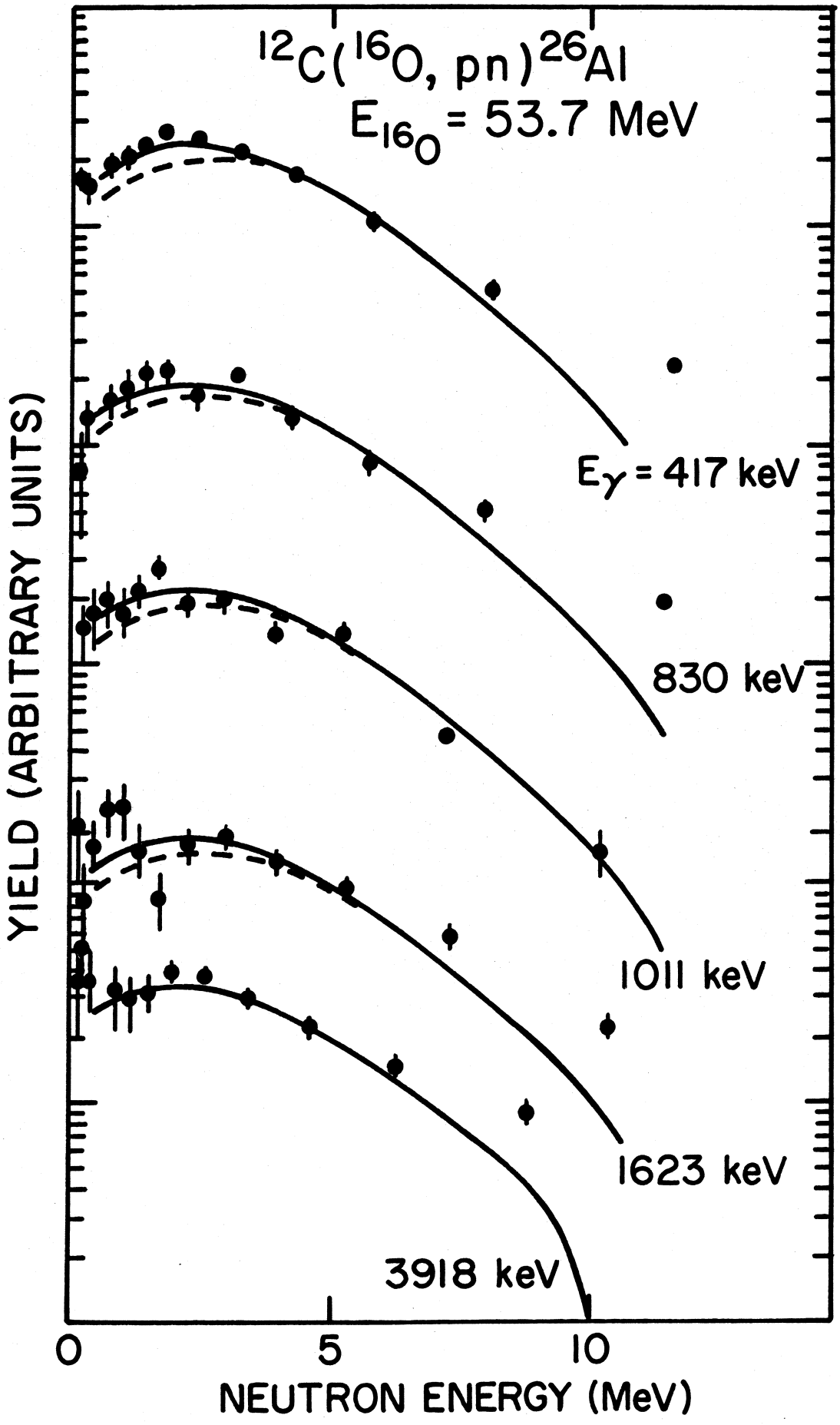
$^{12}C(^{16}O, pn)^{26}Al$
$E_{^{16}O}$ = 53.7 MeV
E_γ = 417 keV
830 keV
1011 keV
1623 keV
3918 keV
YIELD (ARBITRARY UNITS)
0
5
10
NEUTRON ENERGY (MeV)

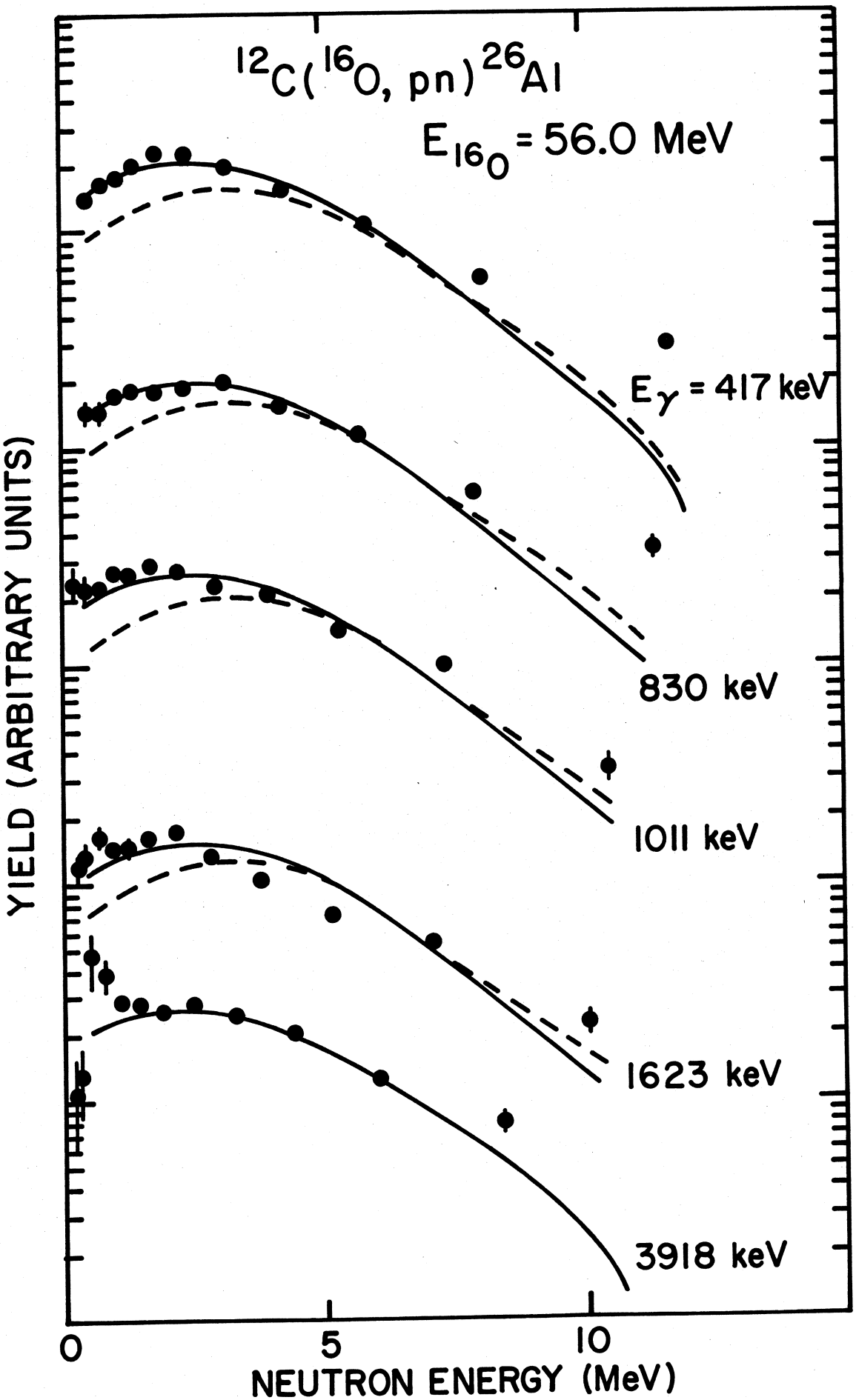
$^{12}C(^{16}O, pn)^{26}Al$
$E_{^{16}O} = 56.0$ MeV
$E_\gamma = 417$ keV
830 keV
1011 keV
1623 keV
3918 keV
YIELD (ARBITRARY UNITS)
0
5
10
NEUTRON ENERGY (MeV)

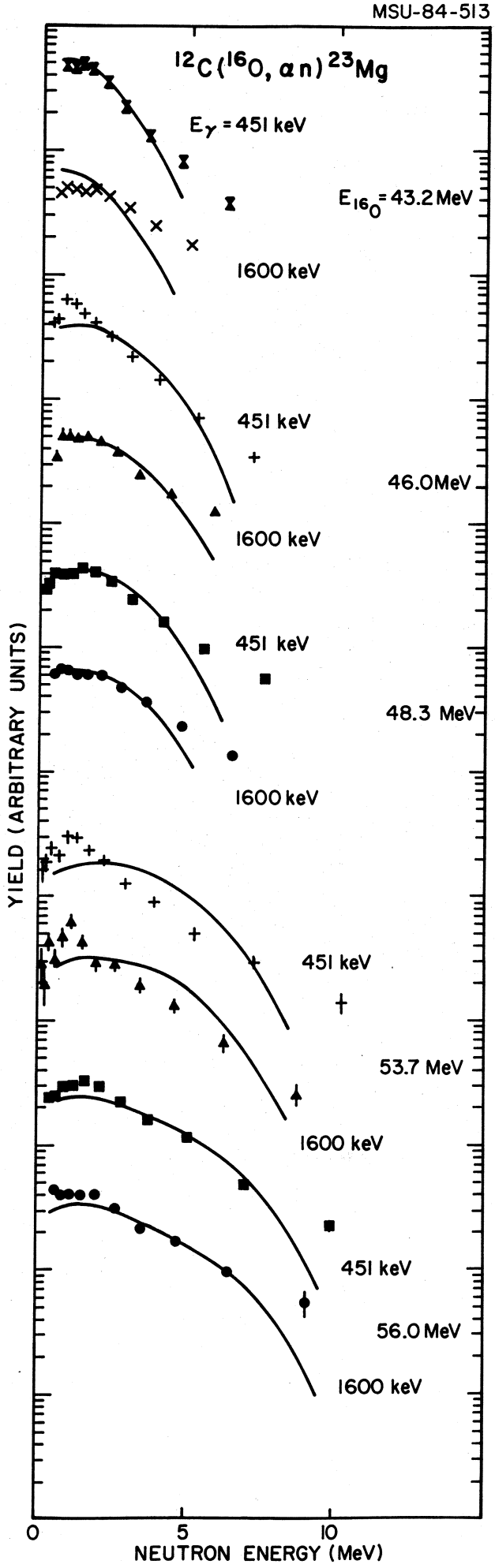
$^{12}C(^{16}O, \alpha n)^{23}Mg$
E_γ = 451 keV
E_{16_O} = 43.2 MeV
1600 keV
451 keV
46.0MeV
1600 keV
451 keV
48.3 MeV
1600 keV
451 keV
53.7 MeV
1600 keV
451 keV
56.0 MeV
1600 keV
YIELD (ARBITRARY UNITS)
0
5
10
NEUTRON ENERGY (MeV)